Tunable Signal Processing Through Modular Control of Transcription Factor Translocation

Nan Hao *et al.*

Science **339**, 460 (2013);
DOI: 10.1126/science.1227299

Research Council (FT110100234), State Key Program for Basic Research (2011CB504701), National Natural Science Foundation of China (81290341), and the Defense Threat Reduction Agency of the USA. The views expressed in this article are those of the authors and do not necessarily reflect the official policy or position of the Department of the Navy, Department of Defense, or the U.S. government. K.A.B.-L. and K.G.F. are contractors for the U.S. government. This work was prepared as part of their official duties. Title 17 U.S.C. §105 provides that "Copyright protection under this title is not available for any work of the United States Government." Title 17 U.S.C. §101 defines a U.S. government work as a work prepared by a military service member or employee of the U.S. government as part of that person's official duties. *P. alecto* and *M. davidii* genomes have been deposited at DNA Data Bank of Japan/European Molecular Biology Laboratory/GenBank under the accession nos. ALWS01000000 and ALWT01000000. Short-read data have been deposited into the Short Read Archive under accession nos. SRA056924 and SRA056925. Raw transcriptome data have been deposited in Gene Expression Omnibus as GSE39933. Tree files and alignments have been submitted to TreeBASE under Study Accession URL: http://purl.org/phylo/treebase/phylows/study/TB2:S13654. We also thank the editor and two anonymous reviewers for their helpful comments and suggestions.
Author contributions: J.W., L.-F.W., G.Z., C.C.B., and K.A.B.-L. conceived the study. M.T., M.L.B., G.A.M., G.C., L.W., and Z.S. prepared the samples. G.Z., Z.H., X.F., Z.X., W.Z., Y. Zhu, X.J., L.Y., J.X., Y.F., Y.C., X.S., Y. Zhang, K.G.F., K.A.B.-L., and J.W. performed genome sequencing, assembly, and annotation. G.Z. and J.W. supervised genome sequencing, assembly, and annotation. G.Z., C.C., Z.H., X.F., J.W.W., Z.X., J.N., W.Z., P.Z., Y. Zhu, M.T., and M.L.B. performed genome analyses. G.Z., Z.H., C.C., and J.W.W. carried out genetic analyses. G.Z., C.C., Z.H., X.F., P.Z., J.N., M.T., J.W.W., M.L.B., and L.-F.W. discussed the data. All authors contributed to data interpretation. C.C. and J.W.W. wrote the paper with significant contributions from G.Z., Z.H., P.Z., J.N., M.T., M.L.B., and L.-F.W. and input from all authors. The authors declare no competing financial interests. Requests for materials should be addressed to the authors for correspondence.

Supplementary Materials
www.sciencemag.org/cgi/content/full/science.1230835/DC1
Materials and Methods
Figs. S1 to S15
Tables S1 to S17
References (*25*–*52*)

28 September 2012; accepted 10 December 2012
Published online 20 December 2012;
10.1126/science.1230835

Tunable Signal Processing Through Modular Control of Transcription Factor Translocation

Nan Hao,[1,2] Bogdan A. Budnik,[1] Jeremy Gunawardena,[3] Erin K. O'Shea[1,2]*

Signaling pathways can induce different dynamics of transcription factor (TF) activation. We explored how TFs process signaling inputs to generate diverse dynamic responses. The budding yeast general stress–responsive TF Msn2 acted as a tunable signal processor that could track, filter, or integrate signals in an input-dependent manner. This tunable signal processing appears to originate from dual regulation of both nuclear import and export by phosphorylation, as mutants with one form of regulation sustained only one signal-processing function. Versatile signal processing by Msn2 is crucial for generating distinct dynamic responses to different natural stresses. Our findings reveal how complex signal-processing functions are integrated into a single molecule and provide a guide for the design of TFs with "programmable" signal-processing functions.

Many transcription factors (TFs) display diverse activation dynamics in response to various external stimuli (*1*–*4*). To investigate how TFs process upstream signals, we studied the *Saccharomyces cerevisiae* general stress–responsive TF Msn2 (*5*). In the absence of stress, Msn2 is phosphorylated by protein kinase A (PKA) and localized to the cytoplasm; in response to stress, Msn2 is dephosphorylated and translocates to the nucleus, where it induces gene expression (*5*).

Natural stresses elicit highly variable dynamics of Msn2 nuclear translocation (Fig. 1A) (*6*, *7*), which are thought to result from oscillatory signaling inputs (presumably PKA activity) (*8*). To study how Msn2 processes oscillatory PKA inputs, we used an engineered yeast strain (*6*) carrying mutations in all three PKA isoforms that enable selective inhibition of PKA activity by a cell-permeable inhibitor, 1-NM-PP1 (*9*). We used this synthetic system and a microfluidics platform (*10*) mounted on a microscope to produce oscillatory inputs of PKA inhibition and monitored translocation of Msn2 to the nucleus. The input amplitude was chosen on the basis of the steady-state amount of Msn2 nuclear localization in response to sustained inputs: high-amplitude input (3 μM 1-NM-PP1) led to maximal nuclear localization of Msn2, whereas low-amplitude input (0.2 μM 1-NM-PP1) induced an intermediate amount of nuclear localization (Fig. 1B, black circles). The pulse duration of oscillatory input was selected on the basis of duration of pulsatile Msn2 nuclear bursts in the physiological response to glucose limitation (*6*). With high-amplitude oscillatory input, each input pulse induced a large amount of nuclear localization (Fig. 1C, left). In contrast, oscillatory input with low amplitude barely elicited any localization responses, although sustained input with the same amplitude led to a half-maximal amount of nuclear localization (Fig. 1C, right). Therefore, Msn2 filters temporal fluctuations of the input in an amplitude-dependent manner such that it tracks high-amplitude inputs, but responds in a limited manner to low-amplitude signals.

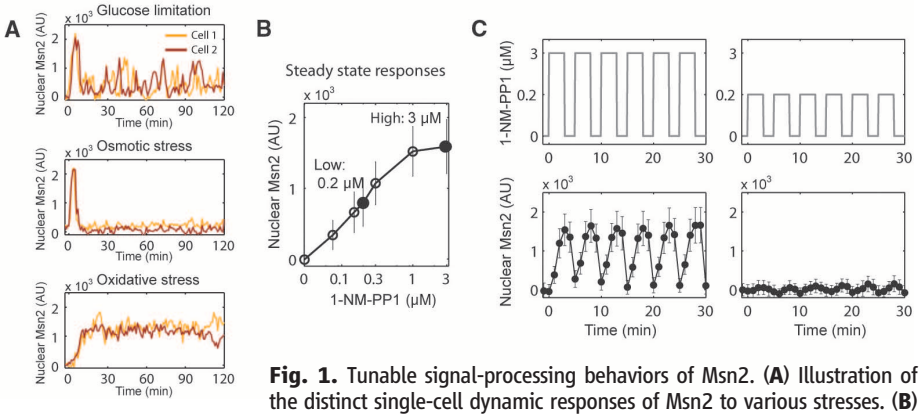

Fig. 1. Tunable signal-processing behaviors of Msn2. (**A**) Illustration of the distinct single-cell dynamic responses of Msn2 to various stresses. (**B**) Steady-state abundance of Msn2 in the nucleus in response to various concentrations of 1-NM-PP1. In response to each concentration of 1-NM-PP1, Msn2 exhibited uniform and stable nuclear localization in single cells and did not exhibit stochastic fluctuations as observed in natural stress responses. Open circles: responses to different concentrations of 1-NM-PP1; closed circles: responses to 3 μM and 0.2 μM 1-NM-PP1, which are used as high- and low-amplitude inputs, respectively, for the following analyses. AU, arbitrary unit. (**C**) Averaged single-cell time traces of Msn2 nuclear translocation (bottom: $n \approx 50$ cells; error bar: single-cell variances) in response to oscillatory inputs with high and low amplitudes (top). (Left) High-amplitude input produced by 3 μM 1-NM-PP1; (right) low-amplitude input produced by 0.2 μM 1-NM-PP1. Pulse duration of 3 min; pulse interval of 2 min. To emphasize the fact that 3 μM 1-NM-PP1 elicits a steady-state response that is about twice the response elicited by 0.2 μM 1-NM-PP1, the top *y* axes are not presented on a linear scale.

[1]Harvard University Faculty of Arts and Sciences Center for Systems Biology, Cambridge, MA 02138, USA. [2]Howard Hughes Medical Institute, Department of Molecular and Cellular Biology, and Department of Chemistry and Chemical Biology, Harvard University, Cambridge, MA 02138, USA. [3]Department of Systems Biology, Harvard Medical School, Boston, MA 02115, USA.

*To whom correspondence should be addressed. E-mail: erin_oshea@harvard.edu

To understand how Msn2 translates signaling inputs into different translocation responses, we characterized Msn2 phosphorylation, which controls nuclear translocation (*5*, *11*). We detected phosphorylation of eight PKA consensus sites, primarily located within the nuclear export signal (NES) and nuclear localization signal (NLS) domains (*11*) (fig. S1). Two sites in the NES (serine at positions S288 and S304) and four sites in the NLS (S582, S620, S625, S633) were functionally important for regulation of nuclear transport (fig. S2).

To intuitively understand the behaviors of the translocation system, we conducted a steady-state analysis that incorporated the separation of time scales for nuclear transport and phosphorylation. For simplicity, we represented regulation of nuclear export and import by phosphorylation of one site in the NES and a second site in the NLS, that act independently of each other (Fig. 2A). We assumed that the slowest time scales occur for nuclear import when the NLS is phosphorylated (k_{in}) and for nuclear export when the NES is unphosphorylated (k_{out}). In contrast, when the NLS is unphosphorylated or when the NES is phosphorylated, nuclear import and export, respectively, both were assumed to occur on faster time scales ($\boldsymbol{k_{in}'}$, $\boldsymbol{k_{out}'}$) (*12*). This scheme gives four phosphoforms with distinct combinations of transport rates (Fig. 2B). Finally, we assumed that phosphorylation and dephosphorylation are fast relative to the translocation time scales (*13*, *14*), so that we could treat transitions between the four phosphoforms, which are triggered by input of PKA inhibition, as effectively instantaneous. PKA and Msn2 phosphatases localize to both the cytoplasm and the nucleus in yeast (*15*–*17*), so Msn2 can be phosphorylated and dephosphorylated in both compartments.

For purposes of illustration, we used a weak and a strong input to represent the amplitude of PKA inhibition (Fig. 2C). Because sites in the

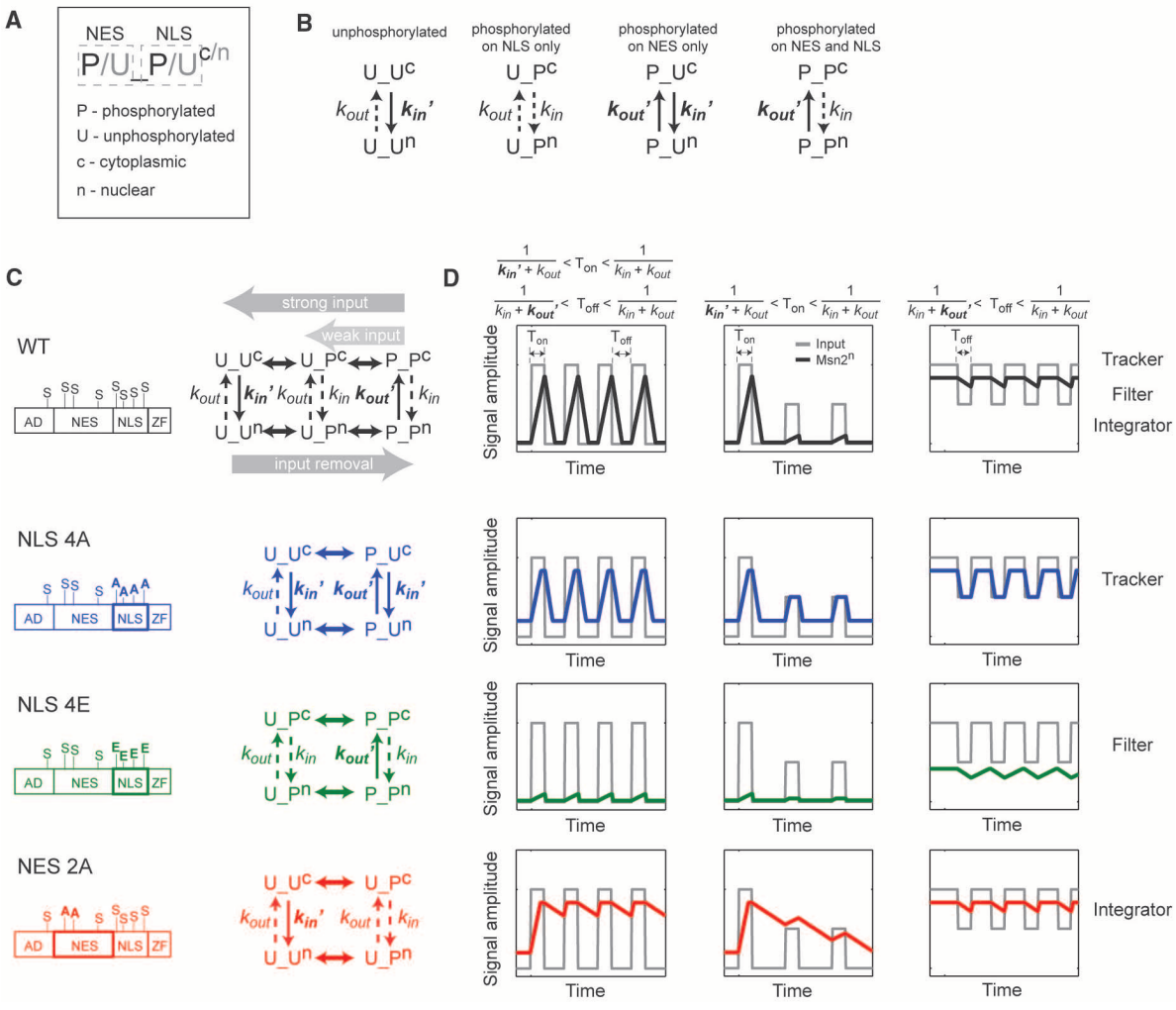

Fig. 2. A theoretical analysis of TF translocation. (**A**) Nomenclature used to define the status of phosphorylation and localization of the TF: for example, the first "P/U": the NES is phosphorylated (P) or unphosphorylated (U); "c/n": superscript shows location in the cytoplasm (c) or nucleus (n). (**B**) Phosphorylation states determine the rate constants of nucleocytoplasmic transport. Unphosphorylated or phosphorylated NES has slow (dashed line) or fast (solid line) nuclear export rates (k_{out}, $\boldsymbol{k_{out}'}$), respectively; unphosphorylated or phosphorylated NLS has fast (solid line) or slow (dashed line) nuclear import rates ($\boldsymbol{k_{in}'}$, k_{in}), respectively. Thus, each phosphoform has a specific combination of nuclear import and export rates. (**C**) The translocation model. (Left) Schematic of WT and phosphosite mutants; (right) model structures and reaction flows (gray arrows) in response to strong or weak inputs and input removal. First row: WT; second row: NLS 4A at S582A, S620A, S625A, and S633A; third row: NLS 4E at S582E, S620E, S625E, and S633E; fourth row: NES 2A at S288A and S304A. We did not specifically study the case in which the NES sites are constitutively phosphorylated because Ser-to-Glu mutants of the NES sites behaved similarly to Ser-to-Ala mutants, which suggests that Glu cannot mimic phosphorylation on NES sites (fig. S2A). (**D**) Predicted responses to various dynamic inputs—first column: oscillatory high-amplitude input, second column: oscillatory input with varied amplitudes, third column: input fluctuating between high and low amplitudes. Color key—black: responses of WT, blue: NLS 4A, green: NLS 4E, red: NES 2A. The ranges of input time scales necessary to generate the predicted responses are determined by the fast and slow time scales of transport rates and are listed above each column. Model output was generated by a steady-state analysis of the translocation system (supplementary materials).

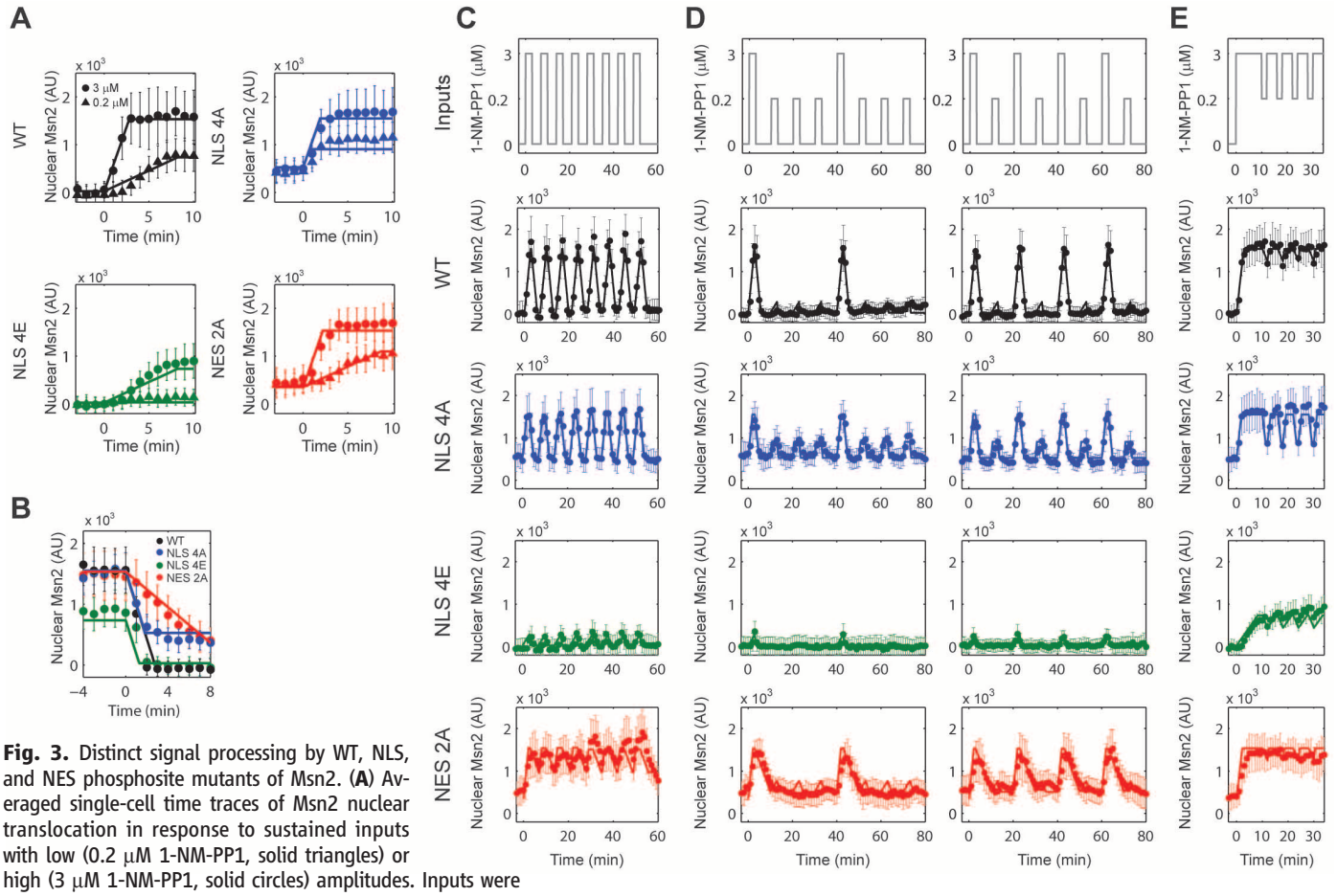

Fig. 3. Distinct signal processing by WT, NLS, and NES phosphosite mutants of Msn2. (**A**) Averaged single-cell time traces of Msn2 nuclear translocation in response to sustained inputs with low (0.2 μM 1-NM-PP1, solid triangles) or high (3 μM 1-NM-PP1, solid circles) amplitudes. Inputs were applied at time point zero. (**B**) Averaged single-cell time traces of Msn2 nuclear translocation in response to removal of high-amplitude input (3 μM 1-NM-PP1). (**C**) Averaged single-cell time traces of Msn2 nuclear translocation in response to oscillatory high-amplitude (3 μM 1-NM-PP1) inputs. Pulse duration of 3 min; pulse interval of 4 min. (**D**) Time traces of Msn2 nuclear translocation in response to oscillatory inputs with a mixture of low- and high-amplitude pulses (0.2 μM 1-NM-PP1 and 3 μM 1-NM-PP1, respectively). (**E**) Time traces of Msn2 nuclear translocation in response to input fluctuating between high (3 μM 1-NM-PP1) and low (0.2 μM 1-NM-PP1) amplitudes. For (A) to (E), data points are averaged single-cell time traces ($n \approx 50$ cells; error bar: single-cell variances). The simple model in Fig. 2 has been fitted to the time trace data in this figure, and the solid lines in (A) to (E) are model fitting results (see supplementary materials, "Model parameters are constrained by experimental data" for details). The dependence of the responses on the time scales of input and transport rates is presented in the supplementary materials, "The relation between time scales of input and time scales of transport rates."

NLS are preferred for PKA phosphorylation over those in the NES (*11*, *18*) (fig. S3), we assumed that weak input (partial inhibition of PKA) would lead to dephosphorylation of only the NES, and the NLS phosphorylated form (U_P^c) would then go to the nucleus with a slow import rate (k_{in}). In contrast, strong input would lead to dephosphorylation of both the NES and NLS, and the fully unphosphorylated form (U_U^n) would be transported into the nucleus with a fast rate (k_{in}'). Upon input removal, the NES and NLS are rephosphorylated and the doubly phosphorylated form (P_P^n) is expected to be exported with a fast export rate (k_{out}') (Fig. 2C, first row). In accordance with this analysis, strong input (3 μM 1-NM-PP1) led to rapid Msn2 translocation, whereas weak input (0.2 μM 1-NM-PP1) resulted in slower translocation, and export is rapid when PKA inhibition is removed [Fig. 3, A and B, wild type (WT)].

We then analyzed how Msn2 might respond to oscillatory inputs. In response to a strong oscillatory input, Msn2 would go in and out of the nucleus with import and export rates (k_{in}', k_{out}') that are fast relative to the input pulse duration and interpulse interval. Hence, Msn2 responded fully to each pulse and tracked the input dynamics (model: Fig. 2D, first row, left; data: Fig. 3C, WT). In response to a weak oscillatory input, Msn2 would enter the nucleus with a slow import rate (k_{in}) relative to the time scale of the input pulse, and therefore, only a small amount of Msn2 entered the nucleus, effectively filtering out low-amplitude signals (model: Fig. 2D, first row, middle; data: Fig. 3D, WT). In response to an input fluctuating between high and low amplitudes, because Msn2 would go out of the nucleus with a slow export rate (k_{out}) relative to the time scale of the interpulse intervals, Msn2 was not fully exported during the interval and integrated the input fluctuations (model: Fig. 2D, first row, right; data: Fig. 3E, WT).

To further test the model and explore the influence of regulation of both import and export on signal processing, we studied cases in which only nuclear import or export, but not both, was regulated by phosphorylation because the functional phosphosites within the NES or NLS were mutated (Figs. 2, C and D, and 3).

In the case in which the NLS sites could not be phosphorylated (NLS 4A), Msn2 would enter the nucleus with a constitutively fast import rate (k_{in}') and go out of the nucleus with a fast export rate (k_{out}') upon input removal (Fig. 2C, second row; data: Fig. 3, A and B, NLS 4A). Hence, in response to oscillatory inputs with high amplitude, low amplitude, or fluctuating between high and low amplitudes, Msn2 would have fast import and export rates; it fully entered the nucleus during a pulse and exited the nucleus during interpulse intervals (model: Fig. 2D, second row; data: Fig. 3, C to E, NLS 4A).

If NLS sites were mutated to mimic constitutive phosphorylation (NLS 4E), Msn2 would enter the nucleus with a constitutively slow im-

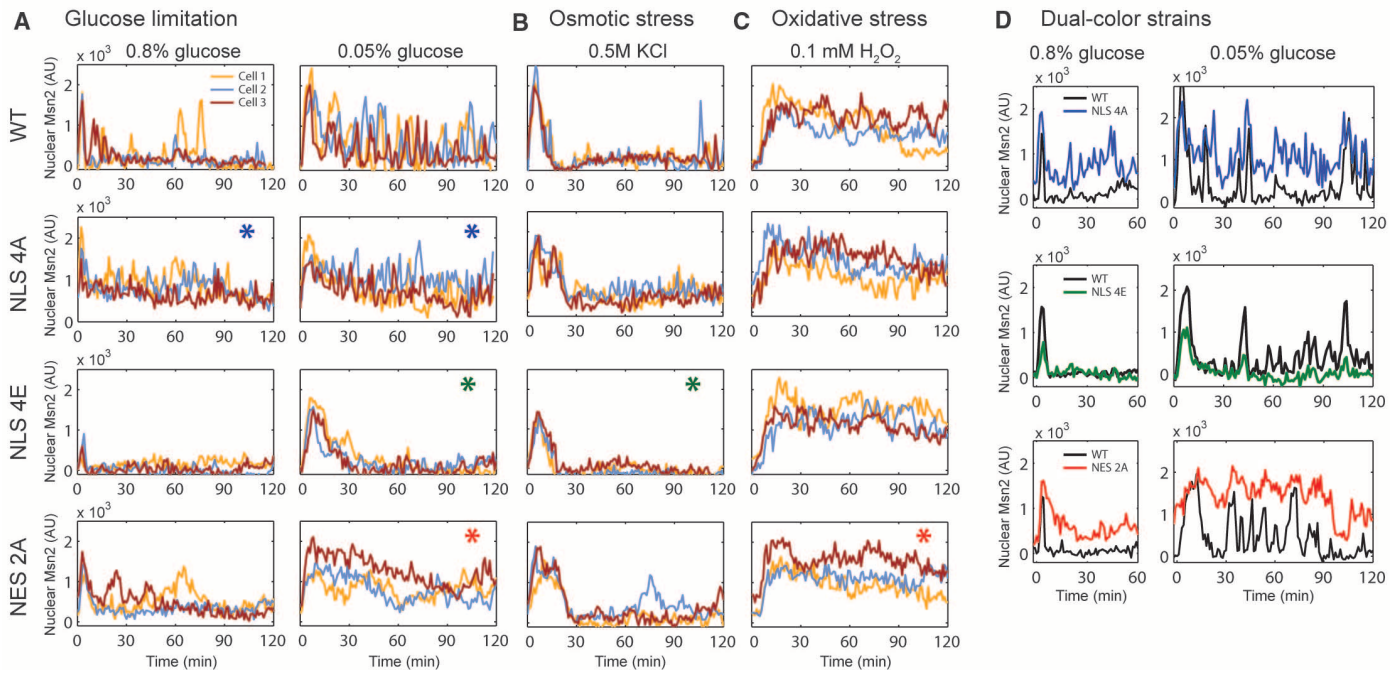

Fig. 4. Distinct responses of WT, NLS, and NES phosphosite mutants of Msn2 to natural stresses. Single-cell responses of WT, NLS 4A, NLS 4E, and NES 2A to glucose limitation (**A**), osmotic stress (**B**), and oxidative stress (**C**) ($n \approx 50$ cells, each stress condition). Representative single-cell time traces of Msn2 nuclear translocation are shown. Asterisks emphasize the conditions under which the mutants fail to distinguish two different stresses. Quantification of the time traces is presented in fig. S4. (**D**) Time traces of WT Msn2-mCherry and mutant Msn2-YFP, monitored in the same cells, in response to glucose limitation (black, WT; blue, NLS 4A; green, NLS 4E; red, NES 2A). More single-cell traces are shown in fig. S5.

port rate (k_{in}) (Fig. 2C, third row; data: Fig. 3A, NLS 4E). In response to oscillatory inputs, when the input duration is short relative to the time scale of the slow import rate, Msn2 went into the nucleus slowly and reached low concentrations (model: Fig. 2D, third row; data: Fig. 3, C to E, NLS 4E).

If NES sites cannot be phosphorylated (NES 2A), Msn2 would exit the nucleus with a constitutively slow export rate (k_{out}) (Fig. 2C, fourth row; data: Fig. 3B, NES 2A). In response to oscillatory inputs with high amplitude, low amplitude or fluctuating between high and low amplitudes, when the interval is short relative to the time scale of the slow export rate, Msn2 would have a slow export rate, could not fully exit the nucleus during intervals, and, therefore, it integrated responses to rapidly changing inputs (model: Fig. 2D, fourth row; data: Fig. 3, C to E, NES 2A). In summary, NLS 4A, NLS 4E, or NES 2A "tracks," "filters," or "integrates" the oscillatory inputs, respectively, whereas WT Msn2 exhibits a combination of all these processing behaviors.

To study the processing of natural stress signals, we monitored WT and mutant Msn2 translocation in response to different stresses (Fig. 4, A to C, and fig. S4). We also monitored the dynamics of WT Msn2-mCherry and mutant Msn2-YFP (fused to yellow fluorescent protein) expressed together in the same cells—this allowed us to directly compare the responses of WT and mutant Msn2 to the same stochastic input signals triggered by natural stress (Fig. 4D and fig. S5). Glucose limitation induced sporadic pulses of rapid nuclear localization of WT Msn2 with frequency regulated by stress intensity; osmotic stress elicited a single pulse of nuclear accumulation; and oxidative stress led to sustained nuclear localization (Fig. 4, A to C, and fig. S4, WT). NLS 4A, which tracks the inputs, was more responsive to inputs and exhibited a high frequency of small rapid bursts of nuclear translocation (Fig. 4D, first row), and thus produced similar response frequencies to low and high levels of glucose limitation (Fig. 4, A to C, second row, marked with blue asterisks; fig. S4D, left, blue circles). By contrast, NLS 4E filtered out the sporadic translocation bursts in response to glucose limitation (Fig. 4D, second row), and therefore, NLS 4E exhibits similar dynamics in response to glucose limitation and osmotic stress (Fig. 4, A to C, third row, marked with green asterisks). NES 2A integrated the sporadic bursts in response to strong glucose limitation (Fig. 4D, third row) and exhibited prolonged nuclear accumulation, similar to that of oxidative stress responses (Fig. 4, A to C, fourth row, marked with red asterisks). Consistent with the analysis of artificial inputs, WT Msn2 and the mutants differed in how they processed signaling inputs triggered by natural stresses and, therefore, generated different responses. WT Msn2 with dual regulation of nuclear import and export generates distinct translocation responses to different stress conditions, whereas the mutants that have only one mode of nuclear transport regulation fail to fully differentiate the different stresses into distinct translocation outputs. Cells may use these diverse TF translocation patterns to induce distinct gene expression programs (*6*) or to elicit different levels of noise in single-cell responses, both of which might be beneficial for survival under stressful conditions.

Nucleocytoplasmic translocation of many mammalian TFs—such as nuclear factors of activated T cells, signal transducers and activators of transcription, and Smads (*19*–*21*)—is controlled by regulation of both their nuclear localization and nuclear export signals. Hence, the proposed dual regulation mechanism may represent a general mechanism for shaping the dynamic behaviors of these TFs. Complex signal-processing behaviors can be achieved by signaling circuits composed of multiple molecules (*22*–*29*). We reveal that a single TF molecule can also mediate sophisticated signal-processing functions by assembling independent functional modules. These functions are "tunable" by phosphorylation at multiple sites in each module and "programmable" by mutating or reassembling functional modules.

References and Notes

1. S. L. Werner, D. Barken, A. Hoffmann, *Science* **309**, 1857 (2005).
2. E. Batchelor, A. Loewer, C. Mock, G. Lahav, *Mol. Syst. Biol.* **7**, 488 (2011).
3. T. K. Lee *et al.*, *Sci. Signal.* **2**, ra65 (2009).
4. J. E. Purvis *et al.*, *Science* **336**, 1440 (2012).
5. W. Görner *et al.*, *Genes Dev.* **12**, 586 (1998).
6. N. Hao, E. K. O'Shea, *Nat. Struct. Mol. Biol.* **19**, 31 (2012).
7. L. Cai, C. K. Dalal, M. B. Elowitz, *Nature* **455**, 485 (2008).

8. C. Garmendia-Torres, A. Goldbeter, M. Jacquet, *Curr. Biol.* **17**, 1044 (2007).
9. A. C. Bishop *et al.*, *Nature* **407**, 395 (2000).
10. P. Hersen, M. N. McClean, L. Mahadevan, S. Ramanathan, *Proc. Natl. Acad. Sci. U.S.A.* **105**, 7165 (2008).
11. W. Görner *et al.*, *EMBO J.* **21**, 135 (2002).
12. A. Komeili, E. K. O'Shea, *Science* **284**, 977 (1999).
13. N. Shulga *et al.*, *J. Cell Biol.* **135**, 329 (1996).
14. J. A. Adams, S. S. Taylor, *J. Biol. Chem.* **268**, 7747 (1993).
15. W. K. Huh *et al.*, *Nature* **425**, 686 (2003).
16. V. Tudisca *et al.*, *Eur. J. Cell Biol.* **89**, 339 (2010).
17. J. M. Tkach *et al.*, *Nat. Cell Biol.* **14**, 966 (2012).
18. G. Neuberger, G. Schneider, F. Eisenhaber, *Biol. Direct* **2**, 1 (2007).
19. H. Okamura *et al.*, *Mol. Cell* **6**, 539 (2000).
20. N. C. Reich, L. Liu, *Nat. Rev. Immunol.* **6**, 602 (2006).
21. X. Chen, L. Xu, *Cell Biosci.* **1**, 40 (2011).
22. S. Levy, M. Kafri, M. Carmi, N. Barkai, *Science* **334**, 1408 (2011).
23. D. M. Longo, A. Hoffmann, L. S. Tsimring, J. Hasty, *Syst. Synth. Biol.* **4**, 15 (2010).
24. W. A. Lim, *Nat. Rev. Mol. Cell Biol.* **11**, 393 (2010).
25. J. C. W. Locke, J. W. Young, M. Fontes, M. J. Hernández Jiménez, M. B. Elowitz, *Science* **334**, 366 (2011).
26. E. C. O'Shaughnessy, S. Palani, J. J. Collins, C. A. Sarkar, *Cell* **144**, 119 (2011).
27. M. Behar, A. Hoffmann, *Curr. Opin. Genet. Dev.* **20**, 684 (2010).
28. M. R. Bennett *et al.*, *Nature* **454**, 1119 (2008).
29. C. J. Bashor, N. C. Helman, S. Yan, W. A. Lim, *Science* **319**, 1539 (2008).

Acknowledgments: We thank A. Murray, P. Cluzel, S. Ramanathan, B. Stern, and M. Rust for comments on the manuscript and S. Mukherji, X. Zhou, A. S. Hansen, and other members of the O'Shea lab for helpful discussions. J.G. is supported by NIH R01 GM081578. E.K.O. is an Investigator of the Howard Hughes Medical Institute.

Supplementary Materials

www.sciencemag.org/cgi/content/full/339/6118/460/DC1
Materials and Methods
Supplementary Text
Figs. S1 to S5
References (*30*–*33*)

11 July 2012; accepted 7 December 2012
10.1126/science.1227299

An Actin-Dependent Step in Mitochondrial Fission Mediated by the ER-Associated Formin INF2

Farida Korobova,[1] Vinay Ramabhadran,[2] Henry N. Higgs[1]*

Mitochondrial fission is fundamentally important to cellular physiology. The dynamin-related protein Drp1 mediates fission, and interaction between mitochondrion and endoplasmic reticulum (ER) enhances fission. However, the mechanism for Drp1 recruitment to mitochondria is unclear, although previous results implicate actin involvement. Here, we found that actin polymerization through ER-localized inverted formin 2 (INF2) was required for efficient mitochondrial fission in mammalian cells. INF2 functioned upstream of Drp1. Actin filaments appeared to accumulate between mitochondria and INF2-enriched ER membranes at constriction sites. Thus, INF2-induced actin filaments may drive initial mitochondrial constriction, which allows Drp1-driven secondary constriction. Because INF2 mutations can lead to Charcot-Marie-Tooth disease, our results provide a potential cellular mechanism for this disease state.

Mitochondrial function extends far beyond that of energy generation, because mitochondria act as sensors of metabolic homeostasis and are key players in cell death pathways (*1*–*4*). The dynamic ability of mitochondria to undergo fission and fusion and to move in cells is important for mitochondrial function, and defects in mitochondrial dynamics are implicated in many neurodegenerative diseases (*5*, *6*). Fission involves oligomerization of dynamin-related protein 1 (Drp1, called Dnm1 in yeast) into a helical ring around the outer mitochondrial membrane, followed by ring constriction. The mechanism for Drp1 recruitment to fission sites, however, is unclear. The diameter of the Drp1 ring is narrower (100 to 130 nm for Dnm1) than an unconstricted mitochondrion (*7*), which suggests that prior constriction may be required. Mitochondrial fission occurs preferentially at endoplasmic reticulum (ER) contact sites, with ER circumscribing mitochondria (*8*). Mitochondria are constricted at these ER contact sites even when Drp1 activity is compromised (*8*). Drp1- and Dnm1-independent constriction is also observed in *Caenorhabditis elegans* (*9*) and budding yeast (*10*), respectively. The mechanism of Drp1-independent mitochondrial constriction is unknown, although actin filaments are implicated in the process (*11*).

Inverted formin 2 (INF2) is a vertebrate formin protein that accelerates both actin polymerization and depolymerization (*12*). In mammalian cells, INF2 exists as two isoforms differing in C-terminal sequence (fig. S1): the prenylated (CAAX) isoform, which is tightly bound to ER (*13*), and the nonCAAX isoform, which is cytoplasmic (*14*). Suppression of INF2-nonCAAX in tissue culture cells causes Golgi dispersal (*14*). In contrast, the cellular function of INF2-CAAX is unclear because its suppression has no apparent effect on ER structure or dynamics (*13*). Physiologically, mutations in INF2 are linked to two human diseases: focal and segmental glomerulosclerosis, a degenerative kidney disease (*15*), and Charcot-Marie-Tooth disease (CMTD), a peripheral neuropathy (*16*).

We decided to test a role for INF2 in controlling mitochondrial size, on the basis of two factors. First, mitochondrial fission takes place at ER contact sites (*8*). Second, other proteins mutated in CMTD affect mitochondrial dynamics (*17*–*19*). INF2 suppression by small interfering RNAs (siRNAs) in either a human osteosarcoma cell line (U2OS) (Fig. 1, A and B, and fig. S2C) or a mouse fibroblast line (NIH 3T3) (fig. S2, A and B) resulted in significant increases in mitochondrial average length and in the percentage of mitochondria over 5 μm. We then tested whether specific suppression of INF2-CAAX in U2OS cells would result in similar mitochondrial elongation. When we treated U2OS cells with two distinct siRNAs that specifically suppressed INF2-CAAX (fig. S3), mitochondrial length increased 2.5 times (Fig. 1, A and B). However, INF2-CAAX depletion did not cause Golgi expansion (fig. S4), an effect attributable to INF2-nonCAAX (*14*). U2OS cells express considerably less INF2-CAAX than NIH 3T3 cells (*14*) but did express detectable levels of INF2-CAAX protein (fig. S3B). Thus, suppression of INF2-CAAX, which localizes to ER, causes an increase in mitochondrial length.

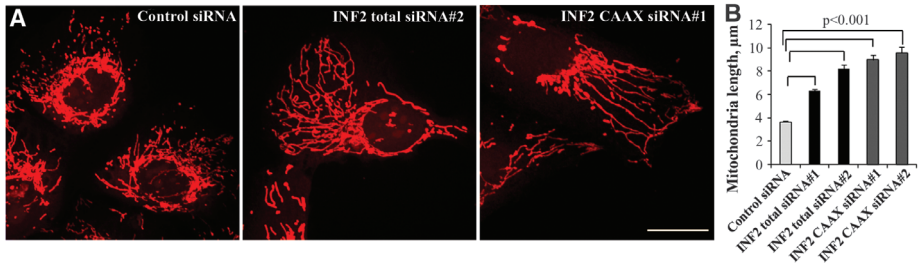

Fig. 1. INF2 suppression increases mitochondrial length. (**A**) Maximum intensity projections of confocal images of MitoTracker-labeled U2OS cells treated with the indicated siRNAs. Scale bar, 20 μm. (**B**) Quantification of mitochondrial lengths. n = 157 to 531 mitochondria. Error bars, SEM.

[1]Department of Biochemistry, Geisel School of Medicine at Dartmouth, Hanover, NH 03755, USA. [2]Howard Hughes Medical Institute, Sackler School of Graduate Biomedical Sciences, Tufts University, Boston, MA 02111, USA.

*To whom correspondence should be addressed. E-mail: henry.higgs@dartmouth.edu